

# A neural network approach for safety and collision avoidance in robotic systems

James H. Graham<sup>a</sup> & Jozef M. Zurada<sup>b</sup>

<sup>a</sup>Computer Science and Engineering, University of Louisville, Louisville, KY 40292, USA

<sup>b</sup>Computer Information Systems, University of Louisville, Louisville, KY 40292, USA

A major factor which has limited the application of robots in industrial and human service applications has been the lack of robust sensing and control algorithms for detection and prevention of collision conditions. This paper discusses an approach to the collision avoidance control of robots using a neural network methodology for the integration of sensory input data from the robot's environment. The paper presents a formulation of the collision avoidance problem using the occupancy grid formulation, and discusses the use of a combination of Dempster-Shafer inference and neural networks in fusing the sensory information and making robot movement decisions. Initial studies have shown this approach to be both robust and computationally tractable in providing enhanced safety capabilities. © 1996 Elsevier Science Limited

## 1 INTRODUCTION

The closely related topics of robot safety and robot collision avoidance in dynamic, nondeterministic environments comprise a significant, and possibly even a crucial, challenge to robotics researchers and practitioners. Many initial applications of robots in industrial settings have been in very simple repetitive tasks, such as material transfer, spot welding, and spray painting, where the robot manipulator is typically anchored to a stationary base, its sequence of movements is reasonably predictable, and its reach is limited. For these applications, standard industrial practices, such as warning signs, barriers, and interlock devices, may be employed to keep untrained personnel away from an operational robot.

As robots begin to be used in applications involving more direct contact with humans, such as service industry applications, it seems obvious that operator training and restriction of access will no longer suffice to maintain adequate conditions of safety, and more active forms of robot safeguarding will have to be developed. This paper presents a multilevel system for improving robot safety by the use of active sensory data from the robot's sensory system. The system includes provisions for preprocessing of the data, integration of data from disparate sensors, and high level decision making.

The subject of collision avoidance in deterministic environments has been extensively studied and reported because of its key importance in path

planning for automatic off-line programming of robot tasks. However, there has been a relatively small amount of research on the problems of robot safety under nondeterministic operating conditions. Research groups at the National Institute for Standards and Technology (NIST),<sup>1</sup> Rensselaer Polytechnic Institute<sup>2</sup> and the University of Louisville<sup>3</sup> have done preliminary investigations into the use of presence sensing devices for robot safety. NIST researchers<sup>4</sup> have also investigated the use of a redundant set of encoders and a separate watchdog safety computer to enforce restricted zones of the workspace. Bennekens & Ramirez<sup>5</sup> have investigated the use of computer vision techniques. Researchers at West Virginia University and the National Institute of Occupational Safety and Health<sup>6</sup> have investigated a combination of light curtains, pressure mats and ultrasonics. Wikman *et al.*<sup>7</sup> have reported an approach to robot collision avoidance using low-level reflex control. Visinsky *et al.*<sup>8</sup> have investigated layered dynamic fault detection, including issues of sensor failure. In Japan, Sugimoto & Kawaguchi<sup>9</sup> have used fault-tree analysis techniques to assess robot hazards. In Finland, Koivo *et al.*<sup>10</sup> have investigated a safety system using light curtains, pressure mats and proximity sensing devices.

This paper is primarily concerned with how robot safety can be improved by the use of active sensory data. There are two principal components to achieving this goal: 1) the processing and reduction of the raw sensory data to extract key features of the workspace; 2) the combination and intelligent use of these

extracted features in making decisions about safe operation. Section 2 provides an analysis of the functional requirements for robot safety and discusses the characteristics of typical sensory devices used for safeguarding. Section 3 discusses an approach toward integration of data from multiple sensors by use of a neural network. Section 4 discusses safety decision making by a neural network, and Section 5 presents a case study using these techniques.

## 2 SYSTEM REQUIREMENTS AND SENSORY DEVICES

A successful robot safety system must satisfy a stringent list of both technical and economic requirements. The primary technical requirement is that it should provide reliable detection of intruders and obstacles, while being highly immune to false alarms. It should be rugged enough to survive an industrial environment, and should provide fail safe operation (i.e., the safety system should fail in a manner so that the robot is disabled). It should be inexpensive relative to the cost of the robot, and should be easy to install and operate. While this paper is primarily concerned with meeting the primary functional objective of accurate detection, it is important to keep in mind the other requirements which play important roles in the industrial application.

In developing a robot safety system, it is necessary to consider the regions over which safety should be

provided, and to specify the appropriate responses within these regions. A good starting point is the three safety regions identified by the National Institute for Standards and Technology<sup>1</sup> as shown in Fig. 1.

The Level I safety region is the area outside the reachable work area of the robot. Safety in this area would typically be achieved in an industrial setting by a physical barrier, such as a woven wire fence, or by a perimeter detection device, such as a photoelectrically sensed light curtain.

The Level II safety region is defined to be the reachable workspace volume of the robot excluding a small volume immediately surrounding the robot itself. Within Level II an intruder is within reach of the robot, but not in imminent danger of being struck.

The Level III safety region is defined to be the volume immediately around the robot. In a simple model this might be a fixed distance, such as 15 centimeters. In a more complex model, this region would vary with the velocity of the robot.

No formal standards have been established for the response to violations of the various safety levels. A reasonable set of responses would be a visual or audible alarm, with possible limitation on the speed of the robot, when an intruder enters the volume protected at Level II. Violations at Level III require an immediate emergency stop.

Figure 2 shows an architecture for a sensory based safety system. The sensors and low level sensory processing will be discussed in the balance of this section, while the higher level functions of sensory integration, obstacle detection and safety decision making will be considered in later sections. In a hierarchically organized safety system, each sensor is connected to a coordinating unit for its particular sensor group. Typical sensor groups would comprise ultrasound ranging devices, passive and active infrared sensors, capacitive and pressure presence sensing, and other units as determined by the specific application, as discussed in the following subsections.

### 2.1 Ultrasound sensors

Ultrasound sensing is based upon producing a high frequency (above 20 kilohertz) sound wave, transmitting this sound wave toward a target, and measuring the time interval until a reflection is detected back at the source. The distance to the reflecting target is linearly related to the observed time delay by the speed of sound in air. Ultrasound sensing is used in commercial intrusion detectors, for focus control in instant cameras, and for industrial ranging and gauging. Ultrasound transducers are relatively lightweight and inexpensive, and sophisticated integrated electronic control units have been developed for them. Transducers with detection ranges of a few centimeters to ten meters are commercially available.

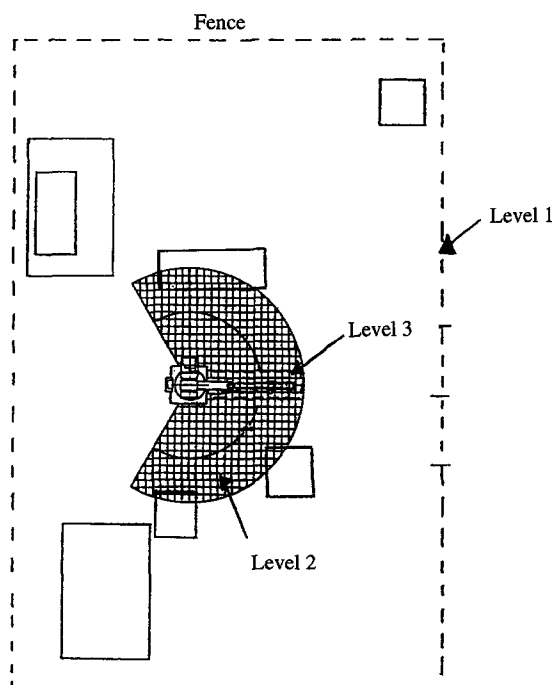


Fig. 1. Safety levels in robot workstation.

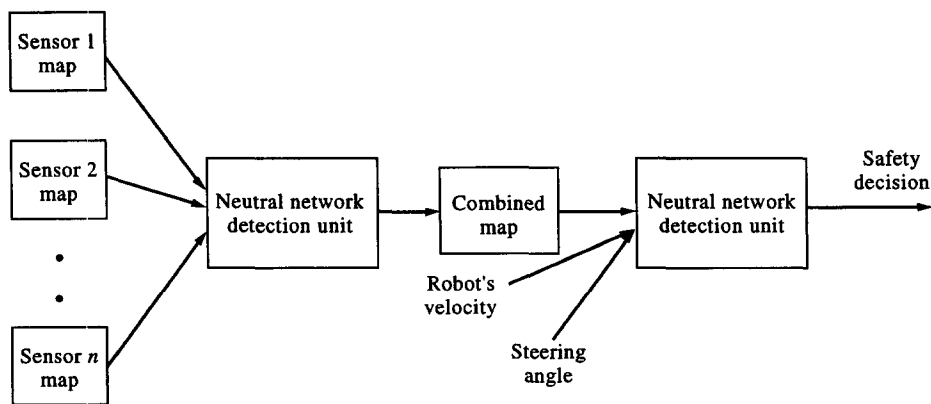


Fig. 2. Architecture for a robot safety system.

## 2.2 Capacitive sensors

Capacitive sensors are currently used in the factory environment as intrusion detection devices around presses and stamping machines to protect workers from inadvertent injury. The sensing unit consists of a radio frequency generator, a control unit, a coupler, and an antenna. An electromagnetic field is produced in the antenna, which acts as one element in a balanced bridge circuit. The control unit is able to detect small changes in the capacitance between the antenna and the ground from this bridge circuit. When an intruder approaches the antenna, the change in dielectric constant in the area surrounding the antenna changes the capacitance. This causes a current flow in the bridge which can be detected and used to trigger an alarm circuit. Typical detection ranges are about forty to fifty centimeters.

## 2.3 Infrared sensors

Humans emit infrared radiation in a well-defined spectral range of about 8–18 microns, and many commercial infrared detectors have been developed that are tuned to these wavelengths. In the pyroelectric detector model, a small ferroelectric crystal is enclosed in a metal container having a small window. Any increase in the radiant energy entering through the window results in the heating of the crystal, and produces an electric current. Most commercial infrared detectors are equipped with sophisticated optical systems which focus different fields of view into the detector window, resulting in a set of detection zones, referred to as 'fingers'. For more reliable detection, differential sensing across a pair of fingers is often used. Typical units have twelve finger pairs, each providing about two degrees of detection, which cover a range of up to twelve meters. Thus, a fairly large area is effectively protected.

## 2.4 Microwave sensing

Velocity sensing microwave units operate on the Doppler principle that when a wave is reflected from a moving object, the frequency of the reflected wave is increased (or decreased) by an amount proportional to the object's speed. These units are used commercially for intrusion detection and to control automatic doors in public buildings. It was determined through experimentation that the microwave lobe pattern is large enough to cover the workspace of a large industrial robot, up to about fifteen meters. Due to this good coverage, and the weight of the unit, it was mounted off the robot. This unit complements the other sensors by providing velocity information about objects in the workspace, as opposed to the presence information provided by other sensing modes. Doppler microwave units do tend to be somewhat sensitive to vibrations, which could reduce the effectiveness in industrial environments.

## 2.5 Other sensory systems

Several other sensory systems have been investigated for use in robot safety applications, including pressure sensitive floor mats, photoelectric light curtains, and computer vision. Floor mats and light curtains are primarily for perimeter penetration detection, and are largely effective at this task. Pressure sensitive skins have been investigated for enhancing collision avoidance in teleoperated robot manipulators by Lumelsky & Cheung.<sup>11</sup> While some preliminary investigation has been performed on the use of computer vision for robot safety, this mode has not been widely used because of cost of computer vision hardware and the general slow speed of image processing algorithms. This situation may change as computer hardware costs come down and computation speed increases.

### 3 INTEGRATION OF SENSORY DATA

#### 3.1 Formulation of the sensory integration model

Formally, let  $S = (S_1, S_2, \dots, S_n)$  be a finite set of sensors which are providing information about conditions within the working space of a robot. Let  $v_i(k)$  be the value returned by sensor  $s_i$  at a particular sampling instant. While  $v_i$  may, in general, be either a continuous or a discrete variable, it will be assumed in this formulation that  $v_i$  is discrete and comes from a finite set of values. Let  $V_i$  be the set of possible values from sensor  $i$  and let  $V = V_1 \cup V_2 \cup \dots \cup V_n$  be the set of all possible sensor values.

Let the set of attributes, about which information is being perceived, be enumerated in a sensory configuration space denoted by  $G = \{g_1, g_2, \dots, g_m\}$ . The attributes measured by sensors may be global properties of the robot workspace, such as ambient temperature, ambient illumination levels, etc., or they may be localized properties, such as the force exerted at the end-effector, or the presence (or absence) of an object at a specified point in the workspace.

Let  $\gamma$  be the function which relates the measured sensor value and the condition of the sensory configuration space.

$$\gamma : V \times S \times G \rightarrow H. \quad (1)$$

Thus, a particular value of  $H$ , say  $h_{ij,k}$ , represents the state of the  $k$ th sensory attribute as reflected by the  $j$ th input value of the  $i$ th sensor. This function provides the mechanism by which the raw sensory value begins to be interpreted into useful information. The function may be as simple as a linear conversion factor or may be a complicated nonlinear operator. In the latter case, it may be desirable to store the function as a lookup table.

An indication of the coupling between sensory systems can be given by the following sensory coupling function:

$$\kappa : S \times G \rightarrow I \quad (2)$$

where  $I_{ij}$  is one if sensor  $i$  provides information about attribute  $j$ , and is zero otherwise. If the matrix implied by the  $\kappa$  function is an identity matrix, then the sensors are measuring unrelated characteristics, and there is no need for sensory fusion.

The goal of the intermediate sensor fusion level is to combine the  $H$  maps generated by the individual sensing units into some sort of decision space  $D$  as indicated by the following:

$$\xi : H_1 \times H_2 \times \dots \times H_n \rightarrow D. \quad (3)$$

As this set of equations suggests, there are two steps in the sensory integration process. The first step involves combining the processed information provided by the individual sensors, represented by the  $H$ 's

of eqn (1). In the following sections these will be represented by occupancy grids or maps, and the first objective will be to construct an integrated map. The second step will be to make a safety decision,  $D$ , based upon the combined sensory map and additional information, such as robot speed and direction. The next subsection provides a formalism for combining the sensory values.

#### 3.2 Dempster-shafer sensory fusion algorithm

Briefly stated, the Dempster-Shafer theory<sup>12</sup> deals with two types of belief, a basic belief (or probability) assignment  $m$  defined upon all subsets of the frame of discernment (sample space) by

$$m : 2^\theta \rightarrow [0,1] \quad (4)$$

subject to the constraints

$$m(\phi) = 0 \text{ and } \sum_{A \subseteq \theta} m(A) = 1 \quad (5)$$

and the derived (or total) belief functions for any event

$$Bel(A) = \sum_{B \subseteq A} m(B). \quad (6)$$

This representation is a good fit to the functional requirements for combining sensory information given in the previous section. The basic belief functions are assigned based upon evidence provided by the sensors. A point type sensor would provide information about a particular grid point, while an area sensor would provide information over several grid points. It is also noted that sensors can provide information about both the presence and absence of objects in the workspace. An ultrasound beam which is reflected provides evidence that an object is at a particular part of the workspace, while a beam that is not reflected provides evidence of freespace in a workspace region.

An advantage of belief functions is that two belief functions  $m_1$  and  $m_2$  defined over the same frame of discernment can be combined by Dempster's rule of direct combination<sup>13</sup> as follows

$$m(A) = \frac{\sum_{A_i \cap B_j = A} m_1(A_i) m_2(B_j)}{1 - \sum_{A_i \cap B_j = \phi} m_1(A_i) m_2(B_j)}. \quad (7)$$

The numerator is the sum of all subset contributions to  $A$  and the denominator acts as a normalization factor by summing all components from empty intersections.

This evidence based approach to sensory fusion has

a number of both qualitative and quantitative advantages as a tool for the coordination of multiple-sensory systems. It has a mathematical rigor which allows it to be readily used with probabilistic estimates of sensory performance. It has a consistent rule for combination which is fully associative and commutative, so that the order of combination is irrelevant. It allows the inclusion of nonconclusive or ambiguous evidence (ignorance) without biasing the results. In short, this approach seems to match well with much of the physical intuition about sensory processing.

The one disadvantage of the evidential approach is the potentially large amount of computation required.<sup>14</sup> The power set assignment of basic beliefs implies a worst case exponential explosion in computation. The following section discusses how this computational limitation can be overcome by using a neural network to approximate the response of the Dempster-Shafer theory.

### 3.3 The neural network detection and integration unit

The neural network detection and sensory integration unit is implemented at an intermediate level of sensory data processing. It is used to implement the Dempster-Shafer combination rule to alleviate the computational complexity of this theory. In particular, neural systems are used to combine basic probability mass functions from different sensors encoded in certainty grids (local maps) into one combined final map of the environment containing potential collision zones with an intruder. The Dempster-Shafer combination rule is used as a response from a teacher in training the network. After the system is taught to combine a representative sample of local maps into a final map, it is able to generalize for situations not encountered in training. In other words, based on the associations developed during the learning phase, it is possible to have the system respond to any combination of local maps with an approximate combined map.

This research has concentrated on the use of a feedforward neural network using a back propagation training methodology.<sup>15</sup> The back propagation algorithm is based on minimization of the error function in the multidimensional weight space, and requires estimation of the gradient of the error using the steepest descent method. Initially, the learning constants are chosen, the activation function for neurons is chosen, and weights are initialized to small random values. The training begins after a single pattern vector  $\mathbf{z}$  is presented at the input, the layers' responses vectors  $\mathbf{y}$  and  $\mathbf{o}$  are computed. Next, the cumulative error of input to output mappings is

computed as the sum over all continuous output errors in the entire training set. In the back propagation step, the error signal vector is determined in the output layer first, and then it is propagated toward the network input nodes, and system weights are adjusted.

The final error value  $E$  for the entire training cycle is computed after each completed pass through a training set  $\{\mathbf{z}_1, \mathbf{z}_2, \dots, \mathbf{z}_p\}$  and set of responses from the teacher  $\{\mathbf{d}_1, \mathbf{d}_2, \dots, \mathbf{d}_p\}$ . The learning procedure stops when the final error value  $E < E_{max}$ . The learning constant  $\eta$  needs to be chosen carefully, so the algorithm converges to a true minimum and does not find a local minimum. A small value for  $\eta$  slows down the training process but guarantees better results. A formal statement of the training algorithm is given in Appendix A. Implementation details and results are discussed in Section 5.

### 4 The neural network decision unit

A neural network decision unit is implemented at the high level of sensory processing and decision making. The neural network accepts the following input: (1) a map containing potential collision zones encoded as belief values into grids, (2) the magnitude of a robot's velocity vector, and (3) robot's steering angle. The neural network decision unit produces one of the following safety decisions: (1) move as intended, (2) slow down, and (3) emergency stop. These decisions are based on computation of the scalar product of two vectors, i.e., the virtual repulsive force vector generated by the obstacle and the robot's velocity vector. The network, in this case, is trained by a human expert who heuristically determines thresholds for safety decisions.

The idea of having obstacles conceptually exerting virtual forces onto a mobile robot was first suggested by Khatib.<sup>16</sup> Krogh & Thorpe<sup>17</sup> further enhanced this concept by taking into account the robot's velocity and its steering angle in the vicinity of obstacles. Borenstein & Koren<sup>18</sup> used the combination of certainty grids and virtual force fields (VFF). The VFF algorithm scans a small square window, for example  $33 \times 33$  cells around or in front of the robot. Each cell inside the window contains a numerical value within the range  $[0,1]$  expressing support for the hypothesis that there is an intruder in the cell. Also, each cell in the window applies a hypothetical repulsive force  $F_r(i,j)$  to the robot located at coordinates  $(x_0, y_0)$ , pushing the robot away from the cell  $(i,j)$ , where  $(i,j)$  are cell coordinates.

$$F_r(i,j) = \frac{F_c B(i,j)}{d^k(i,j)} \left( \frac{x_i - x_0}{d(i,j)} x + \frac{y_j - y_0}{d(i,j)} y \right) \quad (8)$$

where:

- $F_c$  -repelling force constant
- $d(i,j)$  -distance between cell  $(i,j)$  and the robot
- $B(i,j)$  -belief in obstacle in cell  $(i,j)$
- $x_0, y_0$  -robot's present coordinates
- $x_i, y_j$  -coordinates of cell  $(i,j)$
- $k$  -constant (usually set to 2)
- $\vec{x}, \vec{y}$  -  $x$  and  $y$  components of a unit vector.

Since the force constant is divided by  $d^k(i,j)$ , occupied cells exert strong repulsive forces when they are in the immediate vicinity of the robot, and weak forces when they are further away.

In order to compute the resultant virtual repulsive force  $F$ , the individual repulsive force vectors  $F_r(i,j)$  must be computed and accumulated vectorially as given in eqn (9) for each nonzero cell inside the window. Summation of repulsive forces from occupied cells makes the robot highly responsive to clusters of filled cells, while almost completely ignoring the isolated cells.

$$F = \sum_{i,j} F_r(i,j). \quad (9)$$

It is assumed that the robot moves with a fixed velocity and steering angle toward the target. This is certainly an acceptable approximation within the 100 milliseconds, or less, between robot safety assessments. It is also reasonable to increase the strength of the repulsive forces when the robot moves toward an obstacle, and reduce it when the robot moves along, or away from, the obstacle. This can be achieved by computing the scalar product  $S$  of two vectors  $F$  and the robot velocity,  $V$ , that is, multiplying the magnitudes of these two vectors by the cosine of the angle  $\phi$  between them as shown in eqn (10). The scalar product is the largest when a robot faces an obstacle ( $\phi = 0^\circ$ ), equal to zero when the robot moves along the obstacle ( $\phi = 90^\circ$ ), and is negative when the robot moves away from the obstacle ( $\phi > 90^\circ$ ).

$$S = |F||V|\cos(\phi). \quad (10)$$

From eqns (8)–(10), it becomes clear that the belief  $B$  in an obstacle in the sensed area, the distance  $d$  from the robot to the obstacle, the obstacle's size  $OS$ , robot's velocity  $V$ , and the angle  $\phi$  between two vectors  $V$  and  $F$  are all embedded in the scalar product  $S$  as given in eqn (11).

$$S = f(B, d, OS, V, \phi). \quad (11)$$

For this initial work, the decision surfaces were chosen to be  $S = 0.7$  and  $S = 1.4$ . The first decision surface separates the outcome 'Move as Intended' from the outcome 'Slow Down', while the second surface separate 'Slow Down' from 'Emergency Stop'. Additional investigation may yield a more analytical

selection for decision surfaces; however, this heuristic selection has been shown to be quite good in practice,<sup>19</sup> and is not a limitation of the neural network approach.

## 5 SIMULATION AND RESULTS

The robot safety architecture described in this paper has been intensively investigated through computer simulation, using sensory input data from earlier safety studies.<sup>3</sup> Details of the simulation and key results from these investigations are presented here. More complete implementation and testing documentation is given in Ref. 19.

### 5.1 Training and testing the integration unit

It is assumed that a two-dimensional ( $11 \times 15$ ) occupancy grid map is the world representation model, as shown in Fig. 3. It is a working envelope of a hypothetical robot. The robot occupies the shaded square. The low level sensory processing electronics supplies the map data to an intermediate level of processing. The data at this level are represented as basic probability mass functions encoded into grids or areas of grids.

In Fig. 3, sensor 1 (S1) and sensor 2 (S2) cover the areas indicated by 1's and 2's, respectively. Each sensor has its own sensing area, and when used it creates its local sensing map. Each grid or the area of grids may represent a hypothesis. According to the principles of the Dempster-Shafer theory, the frame of discernment  $\Theta$  consists of all the grids in the workspace. For all cases described, the neural network contains 60 and 165 neurons in the hidden and output layer, respectively, and is trained by the back

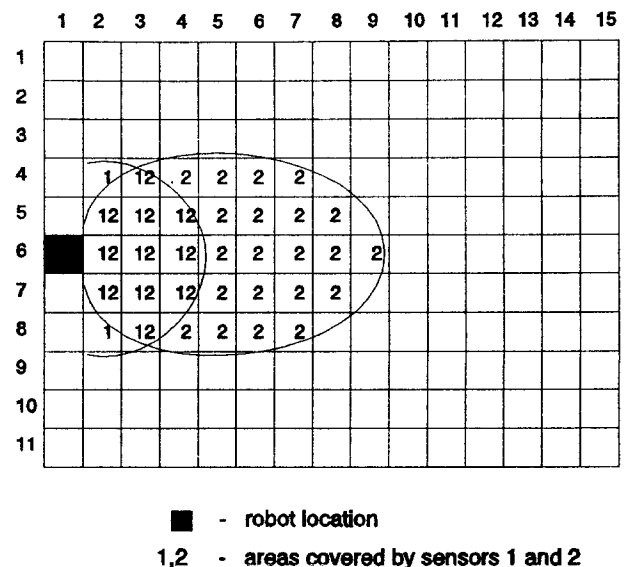


Fig. 3. Areas covered by sensors in grid formulation.

propagation algorithm listed in Appendix A. In the output layer, each neuron is assigned to one grid (cell) in the  $(11 \times 15)$  workspace. The number of training

patterns varies from 300 to 1500, and the neural network is always tested for 300 test cases.

During training for the two sensor case, the neural network accepts, on input six randomly generated probability numbers  $m1(Int)$ ,  $m1(NoInt)$ ,  $m1(\Theta)$  and  $m2(Int)$ ,  $m2(NoInt)$ ,  $m2(\Theta)$  from the training set. These numbers indicate support for the hypotheses described earlier, with  $m1(\Theta)$  and  $m2(\Theta)$  representing any evidence which can not be ascribed to any hypothesis. In addition, the input is augmented by a dummy value of -1. Each six-tuple constitutes a training pattern, and it contains 2 three-tuples. For each six-tuple, the program computes combined beliefs in an intruder at the intersections mentioned above using the Dempster-Shafer theory and its combination rule, as discussed in Section 3.2. The beliefs are then scaled, if needed, by the beliefs assigned to empty intersections. In other words, for each six-tuple, on input, an  $(11 \times 15)$  true map of the environment containing beliefs in grid areas is created and used as a response from a teacher. This true map is compared with the map computed by a neural network, and the differences between the two maps are passed back to the neural network to modify its weights.

After training is finished, the feedback from the Dempster-Shafer teacher is removed, and 300 test cases, which have not previously been used for training, are presented on input, one at a time. Figure 4 shows the neural network map and the exact map for one test case. As mentioned previously, the grid elements represent the basic belief values, after application of the Dempster-Shafer combination rule. Grid elements outside the sensed area are considered to represent an unknown condition. Any uncommitted evidence is assigned to the entire frame of discernment. Examination of this test case shows that, although the network produces approximate results, they are very close to the true results. The response time of the neural network measured on the 90 MHz P5 microprocessor has been measured as 4.7 ms.

The network's overall performance is measured by two criteria:

1. the root mean squared error RMSE defined as

$$RMSE = 100 \frac{1}{NK} \sqrt{\sum_{i=1}^K \sum_{j=1}^N (O_{ij} - D_{ij})^2} [\%] \quad (12)$$

where  $K = 165$  is the total number of grids in the workspace,  $N = 300$  is the number of test cases,  $O_{ij}$  represent probability values in grids generated by the neural network, and  $D_{ij}$  represent true probability values in grids computed using the Dempster-Shafer theory, and

2. the maximum linear error  $MLE$ , defined as

$$MLE_j = \max_i |O_{ij} - D_{ij}|, \quad (13)$$

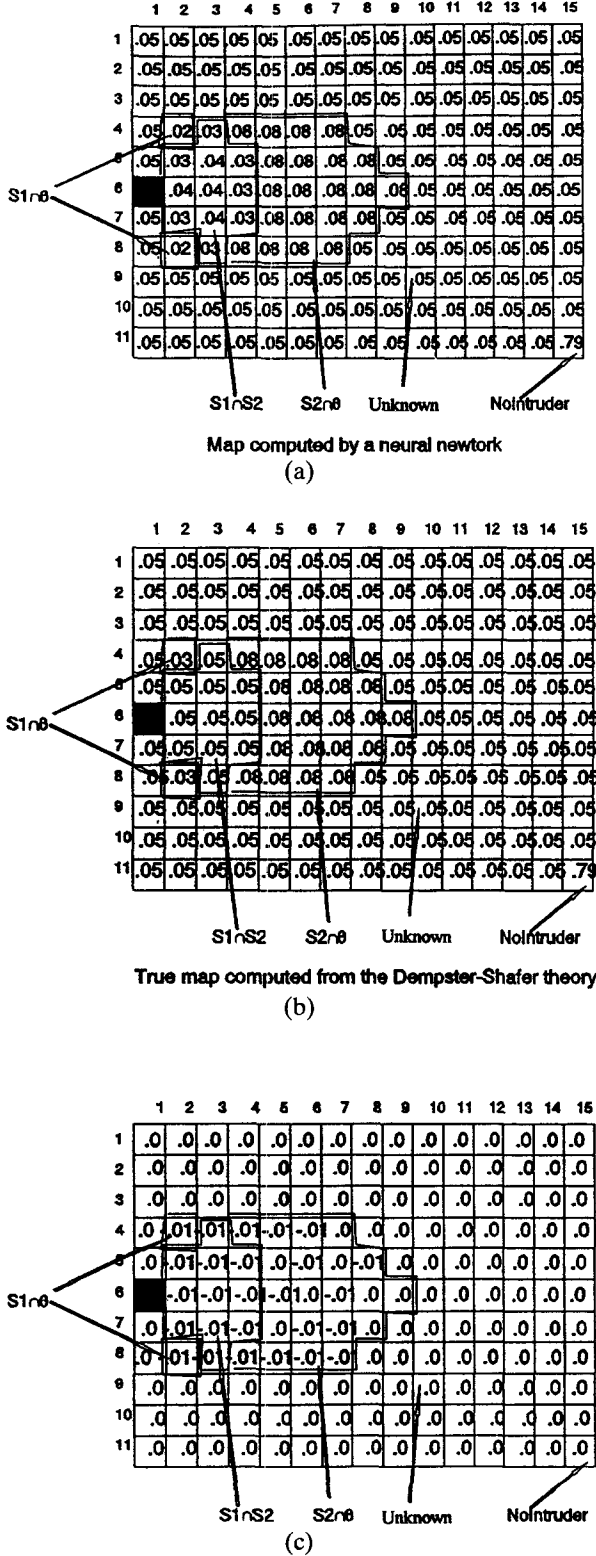


Fig. 4. Test case for detection unit showing (a) beliefs computed by neural network (b) beliefs computed by the Dempster-Shafer theory (c) differences between the two approaches.

between the approximate neural network output and the Dempster-Shafer true output for each map computed for each test case.

For 900 training patterns, the *RMSE* was 0.002%. The distribution of the maximum linear error is shown in Fig. 5. One can easily notice that the maximum linear error is very close to zero for the large majority of the test cases. For eighty-six per cent of the cases the *MLE* is less than or equal to 0.012 and it is less than or equal to 0.048 for ninety-six per cent of the cases. There were only two outliers, with *MLE* greater than 0.048, in the entire data set.

The detection unit was also tested for three and four sensor cases. For the three sensor case, the network accepts on input nine-tuples. Each nine-tuple contains 3 three-tuples, and each three-tuple contains randomly generated probability numbers representing support for beliefs in an intruder, no intruder, and  $\Theta$ , in the area sensed by sensor 1, sensor 2, and sensor 3, respectively. The neural network was trained for 1200 training patterns. The performance of the network is tested, as before, by submitting on its input 300 randomly generated nine-tuples, different from those used for training. The *RMSE* was 0.003%, and the *MLE* was less than 0.05 for 98.33% of test cases with only five outliers being greater than 0.05. For the four sensor case, the neural network was trained for 1500 training patterns. The *RMSE* was 0.002% per grid and the *MLE* was less than 0.06 for 97% of test cases. In summary, the network performs remarkably well producing almost perfect mapping for a vast majority of test cases, and the average measured response time was 5 milliseconds, which is quite acceptable for real-time performance.

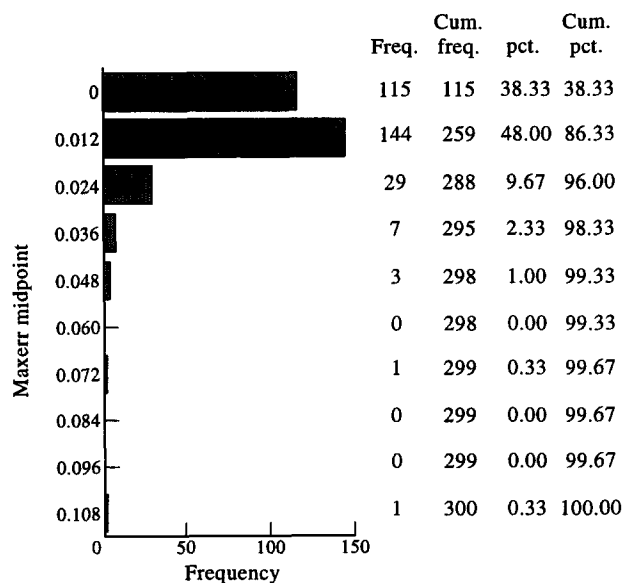


Fig. 5. Distribution of maximum linear error for detection unit.

5.2 Training and testing the decision unit

In this part of the study, a two-dimensional grid world model representation of the size (11×11) feet was used with a robot, indicated by an *R*, located at coordinates (6,1) in Fig. 6. The obstacles have squared shape with sizes 2×2 through 6×6 feet, and they appear randomly, one at a time, at different distances from the robot. The belief *B* in the obstacle is contained within the range [0,1]. The maximum angle  $\phi$  between vectors *F* and *V* is assumed to be 120°, and the robot's velocity varies from 0 to 3 ft/sec.

During training, the neural network accepts, on input, a map with robot position and collision zones, the magnitude of the robot's velocity vector *V* and its steering angle  $\psi$ . All these values are generated at random, and constitute a training pattern. From the robot and obstacle positions, and the value of the belief in the obstacle, the program computes the components of the virtual force vector  $F_r(i,j)$  generated by each grid element. These forces are then accumulated vectorially to produce a resultant virtual force expressed by the magnitude (length)  $|F|$  and the direction (angle)  $\alpha$ . Given the robot's velocity and its steering angle, the scalar product *S* is then computed. For each training pattern on input, the true output (response from a teacher) is determined as follows: (1) if the value of the scalar product *S* is within the range (-6.0,0.7), the three-tuple output is (1,0,0), and it corresponds to the decision 'move as intended', (2) if the value of the scalar product *S* is within the range (0.7,1.4), the three-tuple output is (0,1,0), and it corresponds to the decision 'slow down', (3) otherwise

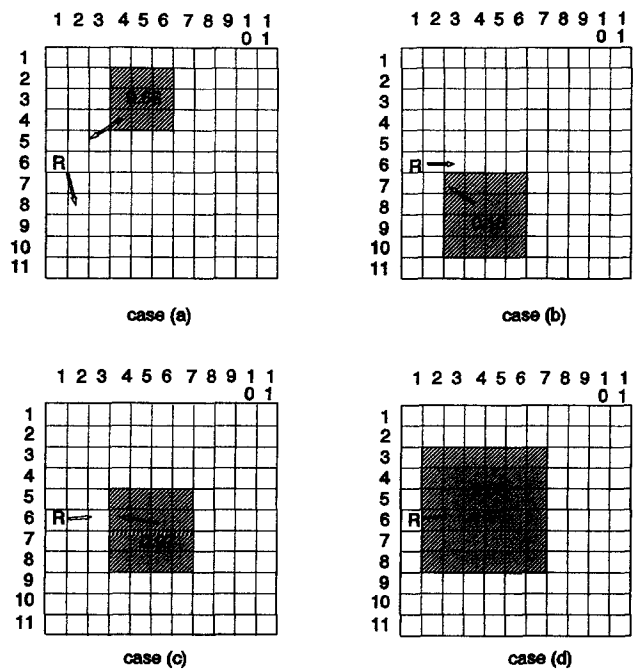


Fig. 6. Four test cases for the neural network decision unit.



the value of  $S \geq 1.4$  yields a decision 'emergency stop', and the three-tuple output is (0,0,1). In each training step, the three-tuple output computed by a neural network is compared with the true three-tuple, and the differences between the two three-tuples are passed back to the neural network to modify its weights.

The neural network contains 124 neurons in each of the input and hidden layers and three neurons in the output layer (corresponding to the three output choices). In the input and hidden layers, each neuron is assigned to one grid in the  $(11 \times 11)$  workspace. Parameters for four training cases, out of 1200, are presented in Table 1. To test the performance of the decision unit, 300 test cases, which have not previously been used for training, are presented on input, one at a time. The neural network decision is determined by the largest of its three outputs. Four test cases, described below, are depicted in Fig. 6. In these test cases, as in the training samples, the beliefs, sizes and positions of the obstacle, as well as robot velocities, were randomly generated.

In case (a), the neural network accepts the map with obstacle of the size  $(3 \times 3)$ ft located at coordinates (2,4). The belief  $B$  in the obstacle is 0.66 and the distance  $D$  to its beginning is about 3.6 feet. The obstacle produces small virtual force  $F = 0.25$  coming from the direction  $\alpha = -36.7^\circ$ . The robot's velocity  $V = 2.7$  ft/sec is very high and robot's steering angle  $\psi = 58^\circ$  is large. The angle  $\phi$  between two vectors  $F$  and  $V$  is  $94.7^\circ$  which means that the robot is moving away from the obstacle. The scalar product computed analytically for this situation amounts to  $-0.06$  which, according to heuristics developed earlier, corresponds to the decision 'move as intended'. For this case, the neural network produces the correct decision 'move as intended'.

In case (b), the obstacle of the size  $(4 \times 4)$ ft is 2.2 feet from the robot and the belief in it is small and equal to 0.18. The robot intends to move with high velocity of 2.8 ft/sec exactly to the right on the map ( $\psi = 1^\circ$ ). The obstacle generates the small virtual force

equal to 0.5 coming from direction of  $34.5^\circ$ . The product of the magnitudes of two vectors is slightly decreased by the  $\phi = 33.5^\circ$  yielding  $S = 0.41$  which corresponds to the decision 'move as intended'. The neural network also classifies this case correctly and produces the decision 'move as intended'.

In case (c), the obstacle of the size  $(4 \times 4)$  almost exactly faces the robot and is 3 feet away from it. The belief  $B = 0.97$  in the obstacle is very high, and robot is moving in the direction of  $-3^\circ$  directly towards the obstacle with moderate velocity of 1.4 ft/sec. The obstacle generates a rather small virtual force of 0.82 units from the direction of  $5.8^\circ$ . The angle  $\phi = 8.8^\circ$  between the two vectors is very small. Although the robot travelling with this speed would move about 2 inches during 100 ms, there is a potential danger close to the robot. The situation produces the value of  $S = 1.13$  which corresponds to the decision 'slow down'. The neural network generates the same decision as well.

In case (d), the obstacle of the size  $(6 \times 6)$ ft is moved slightly upwards relative to the robot and is one foot away from it. The belief  $B = 0.58$  in the obstacle is moderate. The robot faces the obstacle and tries to move almost exactly towards it. The robot's velocity  $V = 2.7$  ft/sec and its steering angle is  $-7^\circ$ . This situation produces large virtual force equal to 2.25 from the direction of  $-3.7^\circ$ . As a result,  $\phi = 3.3^\circ$  and  $S = 1.57$  which corresponds to intuitively correct decision 'emergency stop'. This decision is indeed produced by the neural network.

Among 300 test cases, 25 misclassifications occurred. In nine cases, the neural network produced a 'slow down' decision when 'move as intended' was expected, and in five cases it generated an 'emergency stop' decision when 'slow down' was expected. Thus, it appears that the neural network approach has a tendency to produce a more conservative safety decision, as will be discussed more fully in the next section. The average response time of the neural network decision unit, measured on the 90 MHz, P5 microprocessor, was 5.6 ms.

**Table 1. Parameters for four training samples for the decision unit**

	Case (a)	Case (b)	Case (c)	Case (d)
Obstacle size $OS$	$(5 \times 5)$	$(5 \times 5)$	$(6 \times 6)$	$(5 \times 5)$
Obstacle at position	(6,3)	(2,3)	(4,4)	(4,3)
Belief $B$	0.98	0.15	0.51	0.81
Velocity vector $V$	2.5ft/s	2.3ft/s	2.9ft/s	1.9ft/s
Steering angle $\psi$	$-58^\circ$	$4.1^\circ$	$-59^\circ$	$55^\circ$
$ F $	1.49	0.23	0.67	1.45
Direction (angle) $\alpha$ of $F$	$23.1^\circ$	$-23.1^\circ$	$4.3^\circ$	$0^\circ$
Angle $\phi$ between $F$ and $V$	$81.1^\circ$	$27.1^\circ$	$63.3^\circ$	$55^\circ$
$ F   V $	3.72	0.53	1.95	2.75
$S =  F   V  \cos(\phi)$	0.57	0.47	0.87	1.58
Response from a teacher	1 0 0 'move as intended'	1 0 0 'move as intended'	0 1 0 'slow down'	0 0 1 'emergency stop'

### 5.3 Evaluation of the combined detection and decision units

To test the performance of the overall system, including both the detection and decision making units, the same 300 test cases (maps), which were used originally to test the detection unit by itself, were presented as inputs to the safety system. The robot's velocity  $V$  and its steering angle  $\psi$  were generated randomly, within the ranges [0,3 ft/sec] and  $[-60^\circ, 60^\circ]$ , respectively. Each map produced by the detection unit of the size  $11 \times 15$  ft is reduced to the size of  $11 \times 11$  ft, and only the areas with beliefs in an intruder are shown. The values assigned to ignorance and belief in no intruder are assumed to be zero.

The performance of the overall safety system was remarkably robust. Among 300 test cases, only 24 misclassifications occurred, for a 92% correct classification rate. In addition, fourteen of the misclassifications were in the direction of the more conservative safety decision. In six cases, the neural network decision unit produced a 'slow down' decision while 'move as intended' was expected, and in eight cases it generated an 'emergency stop' decision while 'slow down' was to be produced. In five cases, the neural network produced a 'move as intended' decision while 'slow down' was expected, and in five cases it produced a 'slow down' decision while 'emergency stop' was to be generated. Thus, it appears that the neural network has the tendency to produce a more conservative, that is, a 'safer' decision. When safety is considered, one may assume that those fourteen 'safer' decisions mentioned above are correct decisions. This assumption would actually increase the accuracy of the system to 97%. It is also worth noting that, in none of the misclassified cases, did the neural network generate an extreme error. It never produced a 'move as intended' decision where 'emergency stop' was expected, or produced an 'emergency stop' where 'move as intended' decision was justified.

The average response time for the combined detection and decision unit neural networks using a 90 MHz P-5 microprocessor system was 10.5 milliseconds, well within real-time requirements.

## 6 CONCLUSIONS

This paper has presented a new approach to the unified design of a sensory based robotics safety system for the current generation of fixed location industrial robots. The key to a robust and reliable safety system design is through modularity. This paper presents a hierarchical design that encompasses sensory processing, fusion of sensory data based upon Dempster-Shafer inference, and the high level safety decision making for multi-level alarming. The sensory

integration and safety decision levels are handled by neural networks to achieve speed and a high degree of accuracy.

Initial simulation results have shown this approach to be both robust and computationally feasible. In one sense the robustness of the safety decision is surprising since a number of approximations are made in creating the sensory integration and decision making models; on the other hand, however, this demonstrates the capability of neural networks to smoothly interpolate over analytically complex computations to yield reasonable results. The simulation results discussed here must, of course, be followed by extensive field trials with actual robot workcells to fully validate the approach, but at this point, this new method for combining sensory data and producing safety decisions looks very promising.

## ACKNOWLEDGEMENT

This work was funded in part under Award U60/CCU410085-01 from the National Institute for Occupational Safety and Health (NIOSH). The contents of this paper are solely the responsibility of the authors, and do not necessarily represent the official views of NIOSH.

## REFERENCES

1. Kilmer, R., Safety sensor systems for industrial robots. In *Proceedings of SME Robots 6 Conference*, 1982, Society of Manufacturing Engineers, Michigan, pp. 479-491.
2. Meagher, J., Derby, S. & Graham, J., Robot safety and collision avoidance. *Professional Safety*, **28** (1983) 14-18.
3. Graham, J., A safety and collision avoidance system for industrial robots. *IEEE Trans. Industrial Applications*, **IA-22** (1986) 195-203.
4. Kilmer, R., McCain, H., Jaberts, M. & Legowik, S., Watchdog safety computer design and implementation. In *Proceedings of SME Robots 8 Conference*, Society of Manufacturing Engineers, Michigan, 1984.
5. Bennekers, B. & Ramirez, C., Robot obstacle avoidance using a camera and a 3-D laser scanner. In *Proceedings of SME Vision 86*, Detroit, MI, 1986, Society of Manufacturing Engineers, Michigan, pp. 2.57-2.65.
6. Sneckenberger, J., Kittiampton, K. & Collins, J., Interfacing safety sensors to industrial robotic workstations. *Sensors*, **5** (1987) 35-37.
7. Wikman, T. S., Branicky, M. S. & Newman, W. S., Reflex collision avoidance: a generalized approach. In *Proceedings of IEEE Intl. Conf. Robotics and Automation*, vol. 3, Atlanta, GA, 2-6 May 1993, pp. 31-36.
8. Visinsky, M. L., Walker, I. D. & Cavallaro, J. R., Layered dynamic fault detection and tolerance for robots. In *Proceedings of IEEE Intl. Conf. Robotics and Automation*, vol. 2, Atlanta, GA, 2-6 May 1993, pp. 180-187.
9. Sugimoto, N. & Kawaguchi, K., Fault tree analysis of hazards created by robots. In *Proceeding of 13th Intl.*

- Symp. Industrial Robots, 1983, Society of Manufacturing Engineers, Michigan, pp. 9.13-9.28.
10. Koivo, H., Malm, T., Suominen, J. & Kuivanen, R., An intelligent safety system for robots and automatic machines. In *Safety, Reliability and Human Factors in Robotic Systems*, (ed. J. Graham) Van Nostrand Reinhold, New York, 1991, pp. 132-147.
  11. Lumelsky, V. J. & Cheung, E., Real-time collision avoidance in teleoperated whole-sensitive robot arm manipulators. *IEEE Trans. Systems, Man, and Cybernetics*, **21** (1993) 194-203.
  12. Shafer, G., *A Mathematical Theory of Evidence*, Princeton Univ., Press, Princeton, NJ, 1976.
  13. Dempster, A., Upper and lower probabilities induced by a multivalued mapping. *Annals Math. Stat.*, **38** (1967) 325-339.
  14. Graham, J. & Smith, P., Computational considerations for robot sensory integration. In *Proceedings of Symposium on Advanced Manufacturing*, Lexington, KY, 26-28 September 1988, pp. 115-118.
  15. Zurada, J. M., *Introduction to Artificial Neural Systems*, West Publishing Co., St. Paul, Minn, 1992.
  16. Khatib, O., Real-time obstacle avoidance for manipulators and mobile robots. In *Proceedings of the IEEE International Conference on Robotics and Automation*, St. Louis, MO, 25-28 March 1985, pp. 500-505.
  17. Krogh, B. H. & Thorpe, C. E., Integrated path planning and dynamic steering control for autonomous vehicles. In *Proceedings of the IEEE International Conference on Robotics and Automation*, San Francisco, CA, 7-10 April 1986, pp. 1664-1669.
  18. Borenstein, J. & Koren, Y., Real-time obstacle avoidance for fast mobile robots. *IEEE Trans. Systems, Man and Cybernetics*, **19** (1989) 1179-1187.
  19. Zurada, J., An investigation of artificial neural networks for sensory integration and decision making in robot safety systems. Ph.D. dissertation, University of Louisville, 1995.

## APPENDIX A

### Neural network training algorithm

This appendix presents the formal back propagation algorithm used for training the multilayer neural networks which are used for the detection/integration unit and the safety decision unit. The basic idea in training is that random training samples will be presented to the network simultaneously with the correct network response. (In the detection case the correct response is calculated by the Dempster-Shafer equations, while in the decision case the decision surfaces are used.) The response of the network is compared to the desired response, and the weights of the neurons are modified based upon the observed error. After a sufficient number of repetitions of the training patterns, the network will stabilize and yield a good approximation to the desired output response.

In step 1, the learning constants are determined, the activation function for neurons is chosen, and weights are initialized to small random values. The learning begins in step 2 after a single pattern vector  $\mathbf{z}$  is presented at the input, the layers' responses vectors  $\mathbf{y}$

and  $\mathbf{o}$  are computed. In step 3, the cumulative error of input to output mappings is computed. This error is a sum over all continuous output errors in the entire training set. In step 4, the error signal vector is determined in the output layer first, and then it is propagated toward the network input nodes. In step 5 and 6, the  $K \times J$  and  $J \times I$  weights are adjusted within the matrices  $\mathbf{W}$  and  $\mathbf{V}$ , respectively. The final error value  $E$  for the entire training cycle is computed after each completed pass through a training set  $\{\mathbf{z}_1, \mathbf{z}_2, \dots, \mathbf{z}_p\}$  and set of responses from the teacher  $\{\mathbf{d}_1, \mathbf{d}_2, \dots, \mathbf{d}_p\}$ . The learning procedure stops when the final error value  $E < E_{max}$ .

Step 1:  $\eta > 0$ ,  $E_{max}$ , and  $\lambda$  chosen. ( $\eta$ -a learning constant,  $\lambda$ -a steepness of the continuous perception activation function  $f(net) = 1/(1 + \exp(\lambda net))$  of the neuron, where  $net$  is a summation node).

Weights  $\mathbf{W}$  and  $\mathbf{V}$  are initialized at small random values;

$\mathbf{W}$  is  $(K \times J)$ ,  $\mathbf{V}$  is  $(J \times I)$ .

$q \leftarrow 1, p \leftarrow 1, E \leftarrow 0$ .

Step 2: Training step starts here

Input is presented and the layers' outputs computed,  $\mathbf{z} \leftarrow \mathbf{z}_p, \mathbf{d} \leftarrow \mathbf{d}_p$ .

$y_j \leftarrow f(\mathbf{v}_j^t \mathbf{z})$ , for  $j = 1, 2, \dots, J-1$

where  $\mathbf{v}_j$ , a column vector, is the  $j$ 'th row of  $\mathbf{V}$ , and

$o_k \leftarrow f(\mathbf{w}_k^t \mathbf{y})$ , for  $k = 1, 2, \dots, K$

where  $\mathbf{w}_k$ , a column vector, is the  $k$ 'th row of  $\mathbf{W}$ .

A superscript  $t$  indicates vectors' transposition.

Step 3: Error value is computed:  $E \leftarrow 1/2(d_k - o_k)^2 + E$ , for  $k = 1, 2, \dots, K$ .

Step 4: Error signal vectors  $\delta_o$  and  $\delta_y$  of both layers are computed.

Vector  $\delta_o$  is  $(K \times 1)$ ,  $\delta_y$  is  $(J \times 1)$ .

The error signal terms of the output layer are

$\delta_{ok} = (d_k - o_k)(1 - o_k)o_k$ , for  $k = 1, 2, \dots, K$ .

The error signal terms of the hidden layer are

$\delta_{yj} = y_j(1 - y_j) \sum_{k=1}^K \delta_{ok} w_{kj}$ , for  $j = 1, 2, \dots, J$ .

Step 5: Output layer weights are adjusted:

$w_{kj} \leftarrow w_{kj} + \eta \delta_{ok} y_j$ , for  $k = 1, 2, \dots, K$  and  $j = 1, 2, \dots, J$ .

Step 6: Hidden layer weights are adjusted:

$v_{ji} \leftarrow v_{ji} + \eta \delta_{yj} z_i$ , for  $j = 1, 2, \dots, J$  and  $i = 1, 2, \dots, I$ .

Step 7: If  $p < P$  then  $p \leftarrow p + 1$ , and go to Step 2.

Step 8: The training cycle is completed.

For  $E < E_{max}$  terminate the training session.

Output weights  $\mathbf{W}$ ,  $\mathbf{V}$ ,  $q$ , and  $E$ . If  $E > E_{max}$ , then  $E \leftarrow 0$ ,  $p \leftarrow 1$ ,  $q \leftarrow q + 1$ , and initiate the new training cycle by going to Step 2.

Given are  $P$  randomized training pairs:

$\{\mathbf{z}_1, \mathbf{d}_1, \mathbf{z}_2, \mathbf{d}_2, \dots, \mathbf{z}_P, \mathbf{d}_P\}$ , where  $\mathbf{z}_i$  is  $(I \times 1)$ ,  $\mathbf{d}_i$  is  $(K \times 1)$ , and  $i = 1, 2, \dots, P$ . The  $i$ 'th component of each  $\mathbf{z}_i$  is of value -1 since input vectors are augmented. Size  $J-1$  of the hidden layer having outputs  $\mathbf{y}$  is selected. The  $J$ 'th component of  $\mathbf{y}$  is of value -1, since hidden layer outputs are also augmented;  $\mathbf{y}$  is  $(J \times 1)$  and  $\mathbf{o}$  is  $(K \times 1)$ . For best results, the  $P$  training patterns should be chosen at random from the training set.